BRL R 1954

BRL

REPORT NO. 1954

EXPERIMENTAL MEASUREMENTS OF THE TURBULENT BOUNDARY LAYER ON A YAWED, SPINNING SLENDER BODY

Walter B. Sturek
James E. Danberg

January 1977

USA BALLISTIC RESEARCH LABORATORIES
ABERDEEN PROVING GROUND, MARYLAND

Destroy this report when it is no longer needed.
Do not return it to the originator.

Secondary distribution of this report by originating or sponsoring activity is prohibited.

Additional copies of this report may be obtained from the National Technical Information Service, U.S. Department of Commerce, Springfield, Virginia 22151.

The findings in this report are not to be construed as an official Department of the Army position, unless so designated by other authorized documents.

UNCLASSIFIED

SECURITY CLASSIFICATION OF THIS PAGE (When Data Entered)

REPORT DOCUMENTATION PAGE

READ INSTRUCTIONS BEFORE COMPLETING FORM

1. REPORT NUMBER: BRL Report No. 1954
2. GOVT ACCESSION NO.
3. RECIPIENT'S CATALOG NUMBER
4. TITLE (and Subtitle): EXPERIMENTAL MEASUREMENTS OF THE TURBULENT BOUNDARY LAYER ON A YAWED, SPINNING SLENDER BODY
5. TYPE OF REPORT & PERIOD COVERED: Final
6. PERFORMING ORG. REPORT NUMBER
7. AUTHOR(s): Walter B. Sturek, James E. Danberg
8. CONTRACT OR GRANT NUMBER(s)
9. PERFORMING ORGANIZATION NAME AND ADDRESS: U.S. Army Ballistic Research Laboratory, Aberdeen Proving Ground, Maryland 21005
10. PROGRAM ELEMENT, PROJECT, TASK AREA & WORK UNIT NUMBERS: 1L161102AH43
11. CONTROLLING OFFICE NAME AND ADDRESS: U.S. Army Materiel Development & Readiness Command, 5001 Eisenhower Avenue, Alexandria, Virginia 22333
12. REPORT DATE: JANUARY 1977
13. NUMBER OF PAGES: 30
14. MONITORING AGENCY NAME & ADDRESS (if different from Controlling Office)
15. SECURITY CLASS. (of this report): Unclassified
15a. DECLASSIFICATION/DOWNGRADING SCHEDULE
16. DISTRIBUTION STATEMENT (of this Report): Approved for public release; distribution unlimited.
17. DISTRIBUTION STATEMENT (of the abstract entered in Block 20, if different from Report)
18. SUPPLEMENTARY NOTES
19. KEY WORDS (Continue on reverse side if necessary and identify by block number):
Supersonic Turbulent Boundary Layer
Law of the Wall
Velocity Profiles
Yawed Body of Revolution
Three-Dimensional Boundary Layer
20. ABSTRACT (Continue on reverse side if necessary and identify by block number):

Experimental measurements of the tripped turbulent boundary layer profile characteristics on a yawed, spinning tangent-ogive-cylinder model are described. The profile measurements were made using a flattened total head probe at 30° increments completely about the azimuthal plane for three longitudinal stations at M = 3, 4 and 10,000 RPM. Wall static pressure measurements were obtained in order to compute velocity profiles from the measured total head pressure. The data have been analyzed according to law of the wall/law of the wake concepts using a least squares fitting technique. The effect→ (Continued)

DD FORM 1 JAN 73 1473 EDITION OF 1 NOV 65 IS OBSOLETE

UNCLASSIFIED

SECURITY CLASSIFICATION OF THIS PAGE (When Data Entered)

20. ABSTRACT (Continued (2A p1473A)

of azimuthal position is revealed in the growth of the wake parameter by a factor of two from the wind to the lee-side. A small but consistent effect of spin is also apparent.

4

(1473B)

TABLE OF CONTENTS

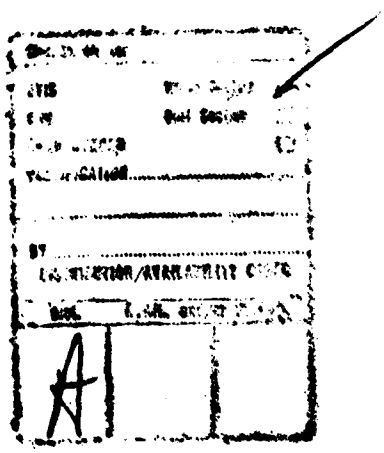

LIST OF ILLUSTRATIONS

I. INTRODUCTION

The U.S. Army Ballistic Research Laboratory is interested in the boundary layer development on yawed, spinning slender bodies of revolution for application to the design of artillery projectiles in general and for gaining further knowledge of the Magnus effect in particular. Reference 1 presents some experimental evidence showing the significant effect that the boundary layer configuration has on the Magnus force experienced by a yawed, spinning body of revolution as well as a discussion of the influence of Magnus on the aerodynamic stability of a spin stabilized projectile. Turbulent boundary layer development over non-spinning bodies of revolution is also of interest to the Army in the aerodynamics of missiles.

Recent advances in computational fluid dynamics have resulted in increased effort toward computation of three dimensional boundary layer development. References 2-5 report three dimensional, laminar and turbulent compressible boundary layer computations for bodies of revolution. Comparisons of the computations to experimental boundary layer profile data have indicated encouraging agreement with the experimental data. This indicates that the numerical techniques are working well; however, comparisons to detailed profile data have only been made for cone models. Comparisons to cone data do not test the computation technique's ability to cope with effects such as longitudinal pressure gradient or changes in wall curvature. Experimental data for comparison to theoretical computations of three dimensional compressible turbulent boundary layer development available in the literature are extremely

---

1. *W. B. Sturek, "Boundary-Layer Distortion on a Spinning Cone," AIAA Journal, Vol. 11, No. 3, March 1973, pp. 395-396.*
2. *T. C. Lin and S. G. Rubin, "A Two-Layer Model for Coupled Three Dimensional Viscous and Inviscid Flow Calculations," AIAA Paper No. 75-853, presented at the AIAA Fluid and Plasma Dynamics Conference, Hartford, Connecticut, June 1975.*
3. *J. C. Adams, Jr., "Finite-Difference Analysis of the Three-Dimensional Turbulent Boundary Layer on a Sharp Cone at Angle of Attack in a Supersonic Flow," AIAA Paper No. 72-186, presented at the AIAA 10th Aerospace Sciences Meeting, San Diego, California, January 1972.*
4. *H. A. Dwyer and B. R. Sanders, "Magnus Forces on Spinning Supersonic Cones--Part I: The Boundary Layer," AIAA Journal, Vol. 14, No. 4, April 1976, pp. 498-504.*
5. *J. E. Harris, "An Implicit Finite-Difference Procedure for Solving the Three-Dimensional Compressible, Laminar, Transitional, and Turbulent Boundary-Layer Equations," NASA SP-347, March 1975, pp. 19-40.*

scarce. References 6 and 7 report experimental measurements of the compressible turbulent boundary layer on yawed cones. Similar experimental measurements for a more general body configuration such as ogive-cylinder are not available in the open literature.

The objective of this experimental effort is to obtain detailed turbulent boundary layer profile data that will be useful for comparisons with theoretical computations. This paper describes measurements of the tripped turbulent boundary layer on a yawed, spinning tangent-ogive-cylinder model. Measurements were made for the model spinning at a rate of 10,000 RPM and also while the model was not spinning. These measurements were made at three longitudinal stations on the cylinder portion of the model for azimuthal stations completely about the circumference of the model in thirty degree increments.

II. THE EXPERIMENT

A. Test Facility

The tests were run in the BRL Supersonic Wind Tunnel No. 1[8]. This is a symmetric, continuous flow, closed circuit facility with a flexible plate nozzle. The test section has a height of 38 cm and a width of 33 cm. The nominal tunnel operating conditions were M = 3.0, $p_o = 0.299 \times 10^6$ Pa, and $T_o = 308$ K. The total pressure was held constant within ± 0.4 percent and the total temperature was controlled within ± 1°K during each individual test run. The Reynolds number based on model length was 7.4×10^6.

B. Model

The model used was a seven caliber long, tangent-ogive-cylinder with a one-caliber ogive section. The diameter of the model was 5.08 cm. A schematic drawing showing the model geometry is given in Figure 1. The model was suspended on ball bearings and an internal air driven turbine was used to drive the model in spin. The model was made of high strength aluminum alloy and was highly polished. The model was

---

6. M. J. Kimbird, "Turbulent Boundary Layer Growth and Separation on a Yawed Cone," AIAA Journal, Vol. 6, No. 12, December 1968, pp. 2410-2416.
7. K. C. Fischer and L. M. Weinstein, "Turbulent Compressible Three-Dimensional Mean Flow Profiles," AIAA Journal, Vol. 12, No. 2, February 1974, pp. 131-132.
8. J. C. McMullen, "Wind Tunnel Testing Facilities at the Ballistic Research Laboratories," BRL Memorandum Report No. 1283, U.S. Army Ballistic Research Laboratories, Aberdeen Proving Ground, Maryland, July 1960. AD 244180.

dynamically balanced to a tolerance of 2.1×10^{-4} (N·m). A boundary layer trip consisting of a 0.64 cm wide band of #80 sand grit was placed 2.5 cm from the tip of the model.

C. Survey Mechanism

The survey mechanism, shown installed with the model in Figure 2, was designed to drive the probe perpendicular to the axis of the model. The probe is positioned by a cam that is rotated using an electric motor mounted within the angle-of-attack crescent. Since the survey mechanism is attached to the angle of attack crescent, the probe is driven perpendicular to the axis of the model for any angle of attack setting. The azimuthal position is determined by selecting predrilled mounting holes placed at 30° increments. The number of azimuthal position changes was kept to a minimum by obtaining data at positive and negative angles of attack.

The survey mechanism was calibrated by using a dial indicator to indicate the displacement of the probe support in thousandths of an inch to establish a table of displacement versus electrical output signal from the probe drive mechanism. In the data reduction procedure divided difference interpolation was used to determine the y position for a given electrical signal. The coordinate system is indicated in Figure 3.

D. Test Procedure

Total head surveys were made of the boundary layer at three longitudinal positions along the cylinder portion of the model for an angle of attack of 4°, M = 3, and for spin rates of zero and 10,000 RPM. The total head probe used had a flattened tip. The probe tip had an opening of 0.076 mm with a lip thickness of 0.025 mm and was 2.5 mm in width. The probe was positioned to measure the pressure along lines parallel to the model axis. A spark shadowgraph showing the model with the total head probe positioned beyond the boundary layer is shown in Figure 4.

The surveys were made by starting the measurements well beyond the edge of the boundary layer--at $y \sim 1.25$ cm whereas the largest δ was about 0.65 cm. The pressure signal from the total head probe was measured using a strain gage transducer that was calibrated within ± 0.25 percent of its full scale range--0-25 psi ($0\text{-}0.172 \times 10^6$ Pa). Measurements were made while holding the probe in a fixed position after allowing approximately thirty seconds for the pressure signal to stabilize. The position of the model surface was detected by electrical signal when the probe contacted the surface of the non-spinning model. Immediately following the survey for the model not spinning, the model was spun to 10,000 RPM and another survey made again starting from well beyond the outer edge of the viscous region. The model spin rate was held constant within ± 50 RPM during the survey using an

automatic control on the air supply to the driving turbine. These surveys were stopped close to, but not touching, the model surface in order to preclude damage to the model surface or the total head probe. Each survey consisted of 35-40 data points.

E. Wall Static Pressure Measurements

Measurements of wall static pressure have been made in order to compute velocity profiles from the measurements of total pressure distribution through the boundary layer. The model used for the wall pressure measurements was a non-spinning model identical in outside dimensions to that used for the boundary layer surveys. Wall pressure taps were located at nine (9) positions on the cylinder portion of the model. The inside diameter of the wall pressure taps was 0.0599 cm. The model and strut support were mounted in the roll head mechanism which allows the model to be rotated in azimuth from $\phi = -90°$ to $\phi = 180°$. Measurements were obtained for angles of attack from 0° to 10° for 10° increments in azimuthal position. The pressure leads from the model were approximately 3 metres in length and were connected to a pressure scanner unit. Each pressure lead was connected to a separate strain gage pressure transducer. These pressure transducers are calibrated within ± 0.25 percent of their full scale range of 0-5 psia (0-.0344 x 10^6 Pa).

F. Data Reduction

The Mach number distribution within the boundary layer has been calculated from measured values of total pressure and wall static pressure using the Rayleigh pitot formula. Velocity and density profiles have been calculated from the Mach number profiles assuming a linear Crocco variation of $(T_t - T_{aw})/(T_{te} - T_{aw})$ vs u/u_e where the adiabatic wall temperature was calculated assuming a recovery factor of 0.88. Integral properties of the boundary layer were calculated by integrating the profile data using a Fortran subroutine which fits a curve to the tabulated data.

An uncertainty is inherent in the profile data due to the probe not being aligned with the local flow direction within the boundary layer. This uncertainty would be greatest near the surface of the model and at longitudinal stations on the forward portion of the model. However, the large gradients present in a turbulent boundary layer would confine the greatest effect of flow angularity to a very small region near the surface which cannot be probed accurately using a total head probe under ideal (two dimensional) conditions. Also, these measurements were obtained for the model at a small angle of attack.

III. DISCUSSION OF THE RESULTS

Examples of the velocity profile data for zero spin are shown in Figures 5, 6, and 7. These profiles clearly show the growth of the boundary layer in the azimuthal and longitudinal directions. Unusual inflection points are noticeable in several of the profiles, particularly in Figure 6 for $\phi = 0°$ and $\phi = 180°$. This behavior suggests the presence of vortices submerged within the boundary layer or a tendency to approach separation. This behavior, however, is not strongly evident at the next downstream station shown in Figure 7. Laser light water vapor flow visualization studies revealed a vortical structure submerged within the boundary layer on the lee side of the model near the base. Boundary layer separation was not indicated until the angle of attack reached 6°. Oil flow visualization was also used in an effort to gain a better understanding of the flow field over the model. Pictures of the oil flow obtained are shown in Figures 8 through 10. The oil flow pattern was obtained by painting the entire model with a thin coating of a mixture of TiO_2 and Dow Corning 200 Fluid. The model, without boundary layer trip, was held non-spinning at 4° angle of attack for about fifteen minutes after flow was started in order for the oil pattern to become fully established. The pictures were made after the tunnel was shut down and with the model at $\alpha = 0°$. The model was positioned at 90° increments in azimuth in order to obtain views over the complete surface of the model. The pictures reveal the presence of high surface shear along the windward ray, wrapping up around the sides of the model as the flow develops toward the base. The unexpected appearance of a slender vortical streamer developing near the tip of the model and wrapping around to the lee-side at about the midlength of the model is also indicated. These oil flow patterns strongly suggest the presence of vortex filaments submerged within the boundary layer on the lee-side.

Wall static pressure measurements for four azimuthal stations at $\alpha = 4°$ are shown in Figure 11. These data indicate that the azimuthal pressure gradient changes from always favorable near the nose of the model to favorable and adverse as the base of the model is approached. The longitudinal pressure gradient changes from mildly favorable on the windside of the model to strongly adverse as the lee-side of the model is approached. The influence of the longitudinal and circumferential adverse pressure gradients is seen in the rapid growth of the lee-side boundary layer profiles shown in Figures 6 and 7.

The integral properties of the boundary layer are shown in Figures 12, 13, and 14. These data indicate that little effect of spin is evident except at the last station. Figure 14 shows that the effect of spin is to decrease the boundary layer thickness on the side where surface spin and the inviscid cross flow are in the same direction; whereas the boundary layer is more thick on the side where the surface spin and inviscid cross flow are in opposite directions.

The growth of the boundary layer in the circumferential and longitudinal directions is shown in the plots of δ^* and θ. The plots of the form factor, H, indicate little effect of longitudinal or circumferential station. The form factor is, however, consistently greater for the spinning model.

IV. LAW OF THE WALL ANALYSIS

A. Profile Characterization

An attempt has been made to gain additional information about the characteristics of the measured velocity profiles using "law of the wall" and "law of the wake" turbulent boundary layer concepts. The procedure used is based on the method proposed in reference 9 where a least square fitting technique is employed to determine certain profile parameters. The form of the assumed profile is based on the work of Coles'[10] in incompressible flow in which the boundary layer is found to have a wall region in which the velocity is dependent on a velocity scale, u_s, and a length scale, ν_w/u_s, and a wake region which is also dependent on u_s but the length scale is a boundary layer thickness, δ_s. The following functional relationship was used in the data reduction:

$$\tilde{u}/u_s = \ln (u_s y/\nu_w) + C_s + 2\,\Pi_s \sin^2 (\pi y/2\delta_s) \; . \qquad (1)$$

law of the wall law of the wake

Compressibility effects are accounted for, at least approximately, using the results of the Prandtl-Van Driest[11] mixing length analysis in which the compressible flow velocity, u, is transformed into an equivalent incompressible form through the relation

---

9. *J. E. Danberg, "A Re-evaluation of Zero Pressure Gradient Compressible Turbulent Boundary Layer Measurements," Proceedings CP-93, AGARD Fluid Dynamics Specialists Meeting on 'Turbulent Shear Flows', 1971.*
10. *D. E. Coles, "The Law of the Wake in Turbulent Boundary Layers," Journal of Fluid Mechanics, Vol. 1, Part 2, 1956, pp. 191-226; also, see D. E. Coles and E. A. Hirst, "Proceedings AFOSR-IFP-Stanford Conference on Computation of Turbulent Boundary Layers--1968," Vol. II, pp. 1-45.*
11. *E. R. Van Driest, "Turbulent Boundary Layers in Compressible Fluids," Journal of Aeronautical Sciences, Vol. 18, No. 3, 1951, pp. 145-160.*

$$\tilde{u} = \int_0^u \sqrt{\rho/\rho_w}\, du \tag{2}$$

which is evaluated numerically from the measured Mach number profiles and assuming: (1) constant pressure across the boundary layer, (2) perfect gas equation of state, (3) adiabatic relationship between Mach number, total and static temperature, and (4) the Crocco temperature-velocity equation

$$(T_t - T_w)/(T_{t_e} - T_w) = \beta\,(u/u_e) + (1 - \beta)(u/u_e)^2$$

$$\beta = (T_{aw} - T_w)/(T_{t_e} - T_w) \tag{3}$$

with a constant recovery factor of .89 used in evaluating the adiabatic wall temperature.

In equation (1) there are four parameters; u_s, C_s, Π_s, and δ_s which are determined so as to minimize the rms deviation between the profile measurements and the analytical curve. It should be noted that the form of the "law of the wall" used here is not valid in the laminar sublayer region near the wall. Data close to the wall which systematically deviate from the semilogarithmic relation are omitted from the fitting procedure. The equation is also not valid when the velocity becomes uniform at the edge of the boundary layer. Only data corresponding to y values less than δ are used in the curve fitting, where δ is defined as the value of y at which the derivative of equation (1), that is $d\tilde{u}/dy$, is zero. The boundary layer thickness, δ, is typically ten percent larger than δ_s.

The more conventional form of equation (1), for example as used by Coles[10], is related to equation (1) when

$$u_s = u_\tau/\kappa \tag{4}$$

where κ = Prandtl's mixing length constant

u_τ = wall shear velocity = $\sqrt{\tau_w/\rho_w}$

As a consequence the usual constant in the logarithmic wall law is related to C_s by

$$C_s = C\kappa + \ln \kappa \qquad (5)$$

The change in definition of these two parameters is desirable for the present purposes because κ cannot be determined solely from velocity profile data unless accurate data in the laminar sublayer is obtained. However, if κ is assumed known ($\kappa \sim .4$ approximately) then equation (4) may be used to determine the wall shear stress.

Equation (1) is found to adequately describe a wide range of two-dimensional turbulent boundary layer measurements except, of course, in the laminar sublayer. Most two-dimensional profiles can be represented in this way with a root-mean-square deviation of less than $\pm .03$ in $\tilde{u}/u_s$. This corresponds to about $\pm .3\%$ of the maximum flow velocity at the edge of the boundary layer which is approximately the error expected in the transducers used for the pressure measurements. The fit of the three-dimensional boundary layers considered here was typically the same with the maximum rms deviation of .09%. Figure 15 illustrates the quality of the fit obtained with the present data. The figure shows the variation of the velocity profiles with azimuthal position for the most rearward station (6 calibers from the nose) on the non-spinning model. The thickening of the boundary layer on the leeward side (180°) is evident as well as a significant increase in the size of the wake region of the profile. The profiles obtained on the spinning model at 10,000 RPM are essentially the same as for the non-spinning case.

B. Azimuthal Distribution of Profile Parameters

In Figure 16 the wake region profile parameter, Π_s, is shown plotted against azimuthal position for the most rearward station (Z/D = 6). The maximum velocity increase relative to the logarithmic law is proportional to Π_s and the leeward side (180°) is more than twice that on the windward side (0°). The level on the windward side is comparable with the accepted incompressible value of $\Pi_s = .55$[12] for zero pressure gradient flow. A survey of compressible flow, zero pressure gradient data indicated a value of $\Pi_s = .81$[9] but the data base included a number of surveys taken on wind tunnel nozzle walls and these contain significant history effects which cause the value of Π_s to vary with facility Mach number[13]. Thus, the value of Π_s on the windward side of

12. *D. E. Coles, "The Turbulent Boundary Layer in a Compressible Fluid," RAND Corp., Report R-403-PR, 1962.*
13. *J. E. Danberg, "Some Supersonic Wind Tunnel Nozzle Boundary Layer Characteristics," BRL Memorandum Report No. 2618, U.S. Army Ballistic Research Laboratories, Aberdeen Proving Ground, Maryland, April 1976. AD A024980.*

the model is essentially that of a zero pressure gradient, two dimensional boundary layer. On the leeward side Π_s is more characteristic of an adverse pressure gradient situation. In addition to the variation of Π_s with azimuthal angle, there is also a small but consistent effect of spin. At 10,000 RPM the curves are slightly displaced in the direction of rotation.

Figure 17 shows the strong variation of the wall region parameter, C_s, with azimuthal position. The general level of C_s on the leeward side is approximately 1.0 which is quite close to the incompressible zero pressure gradient value of 1.16 ($C = 5.5$, $\kappa = 0.4$). On the windward side C_s is over three times larger. Zero pressure gradient data from a number of sources[9] indicate a mean value of 1.8 from both flat plate and nozzle wall results but with a large degree of scatter which may indicate that history effects are important. These results as well as those for Π_s show that the character of the turbulent boundary layer on the leeward side between 120° and 240° is quite different from that on the windward side of the model.

V. SUMMARY

An experimental effort has been described in which measurements of the three-dimensional turbulent boundary layer have been obtained for a yawed, spinning slender body of revolution in supersonic flow. Wall static pressure measurements were made on a non-spinning model to enable velocity profiles to be computed from the total head surveys of the boundary layer. The measurements provide a unique set of flow field data for comparison with theoretical computations of boundary layer development and inviscid flow fields. Several observations made upon examination of these data are listed below.

(1) A spin rate of 10,000 RPM has only a slight effect on the measured boundary layer profile characteristics for the tripped turbulent boundary layer.

(2) The circumferential velocity component experiences a favorable pressure gradient from the wind to the lee-side at forward positions on the model; but the pressure gradient changes from favorable to adverse at rearward stations as the lee-side is approached.

(3) A least square curve fitting technique has been used to characterize the measured velocity profiles in terms of four parameters which are related to the "law of the wall" and "law of the wake" regions of a turbulent boundary layer. The wake parameter, Π_s, and the wall parameter, C_s, show strong variation around the model associated

with the effects of angle of attack. One effect of spin rate is found to be a shift in the wake profile parameter distribution in the direction of spin.

REFERENCES

1. W. B. Sturek, "Boundary-Layer Distortion on a Spinning Cone," *AIAA Journal*, Vol. 11, No. 3, March 1973, pp. 395-396.

2. T. C. Lin and S. G. Rubin, "A Two-Layer Model for Coupled Three Dimensional Viscous and Inviscid Flow Calculations," AIAA Paper No. 75-853, presented at the AIAA Fluid and Plasma Dynamics Conference, Hartford, Connecticut, June 1975.

3. J. C. Adams, Jr., "Finite-Difference Analysis of the Three-Dimensional Turbulent Boundary Layer on a Sharp Cone at Angle of Attack in a Supersonic Flow," AIAA Paper No. 72-186, presented at the AIAA 10th Aerospace Sciences Meeting, San Diego, California, January 1972.

4. H. A. Dwyer and B. R. Sanders, "Magnus Forces on Spinning Supersonic Cones--Part I: The Boundary Layer," *AIAA Journal*, Vol. 14, No. 4, April 1976, pp. 498-504.

5. J. E. Harris, "An Implicit Finite-Difference Procedure for Solving the Three-Dimensional Compressible Laminar, Transitional, and Turbulent Boundary-Layer Equations," NASA SP-347, March 1975, pp. 19-40.

6. W. J. Rainbird, "Turbulent Boundary Layer Growth and Separation on a Yawed Cone," *AIAA Journal*, Vol. 6, No. 12, December 1968, pp. 2410-2416.

7. M. C. Fischer and L. M. Weinstein, "Turbulent Compressible Three-Dimensional Mean Flow Profiles," *AIAA Journal*, Vol. 12, No. 2, February 1974, pp. 131-132.

8. J. C. McMullen, "Wind Tunnel Testing Facilities at the Ballistic Research Laboratories," BRL Memorandum Report No. 1292, U.S. Army Ballistic Research Laboratories, Aberdeen Proving Ground, Maryland, July 1960. AD 244180.

9. J. E. Danberg, "A Re-evaluation of Zero Pressure Gradient Compressible Turbulent Boundary Layer Measurements," Proceedings CP-93, AGARD Fluid Dynamics Specialists Meeting on 'Turbulent Shear Flows', 1971.

10. D. E. Coles, "The Law of the Wake in Turbulent Boundary Layers," *Journal of Fluid Mechanics*, Vol. 1, Part 2, 1956, pp. 191-226; also, see D. E. Coles and E. A. Hirst, "Proceedings AFOSR-IFP-Stanford Conference on Computation of Turbulent Boundary Layers--1968," Vol. II, pp. 1-45.

REFERENCES (Continued)

11. E. R. Van Driest, "Turbulent Boundary Layers in Compressible Fluids," *Journal of Aeronautical Sciences*, Vol. 18, No. 3, 1951, pp. 145-160.

12. D. E. Coles, "The Turbulent Boundary Layer in a Compressible Fluid," RAND Corp., Report R-403-PR, 1962.

13. J. E. Danberg, "Some Supersonic Wind Tunnel Nozzle Boundary Layer Characteristics," BRL Memorandum Report No. 2618, U.S. Army Ballistic Research Laboratories, Aberdeen Proving Ground, Maryland, April 1976. AD A024980.

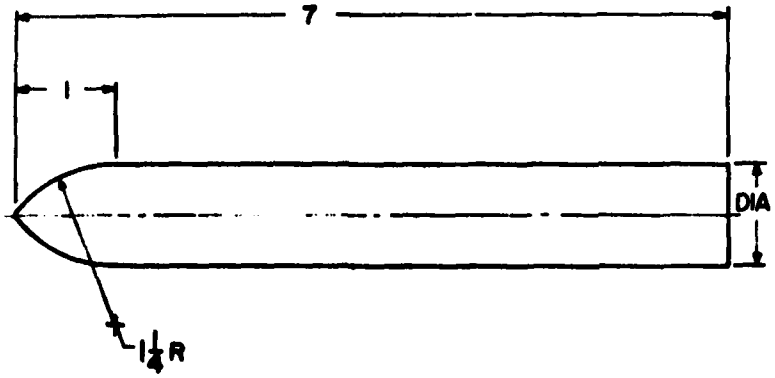

NOTE: ALL DIMENSIONS IN CALIBERS
DIA = 5.08 cm

Figure 1. Model Geometry

Figure 2. Model Installation With Survey Mechanism

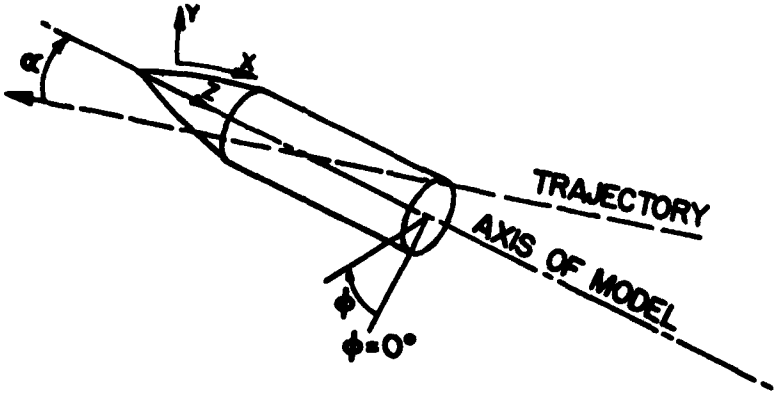

Figure 3. Coordinate System

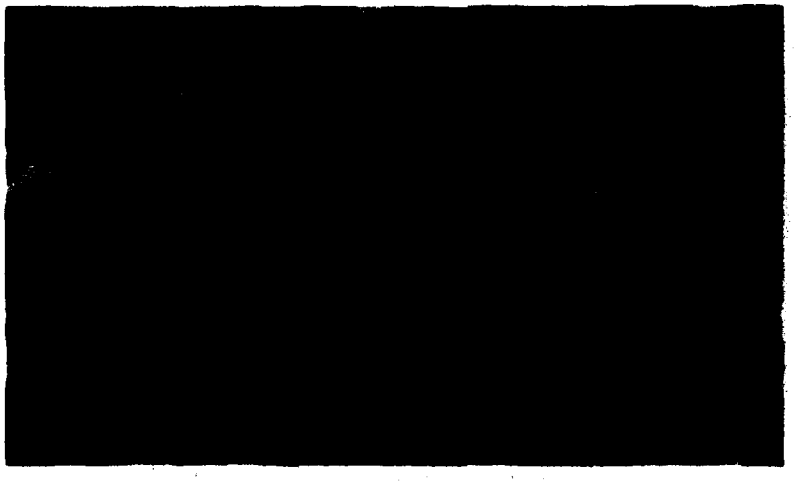

Figure 4. Spark Shadowgraph of Flow, M = 3, α = 4°

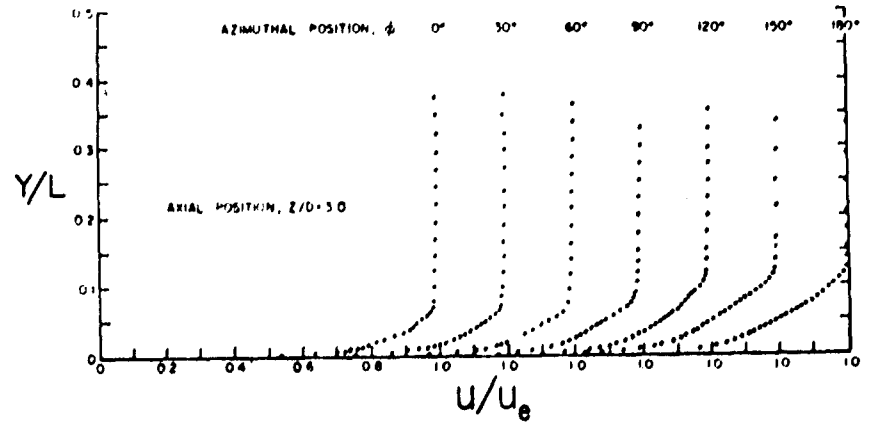

Figure 5. Velocity Profiles, M = 3, α = 4°, Z/D = 3.0, Zero Spin

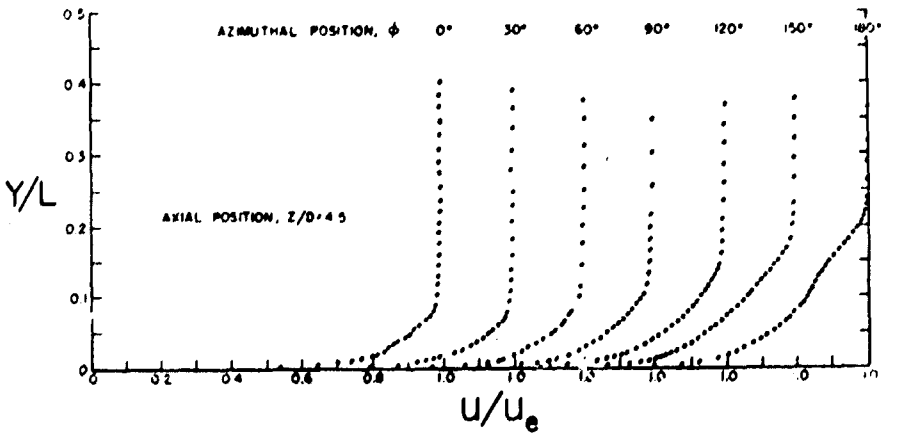

Figure 6. Velocity Profiles, M = 3, α = 4°, Z/D = 4.5, Zero Spin

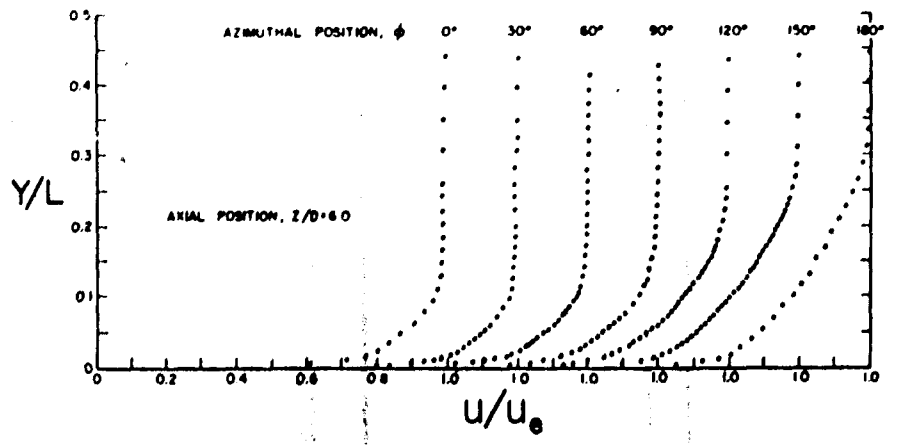

Figure 7. Velocity Profiles, M = 3, α = 4°, Z/D = 6.0, Zero Spin

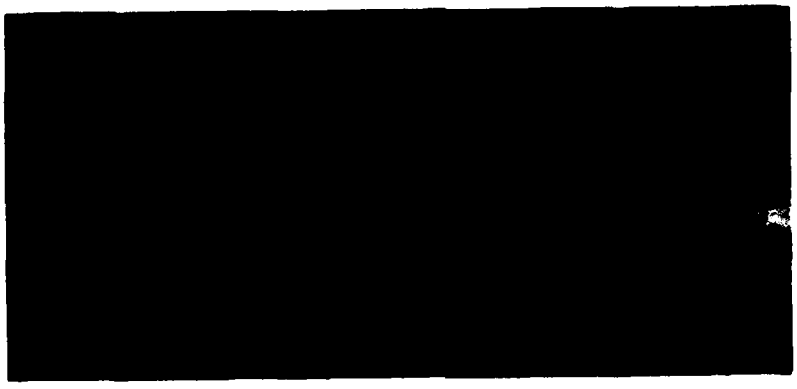

Figure 8. Oil Flow Visualization, M = 3, α = 4°, ϕ = 0°

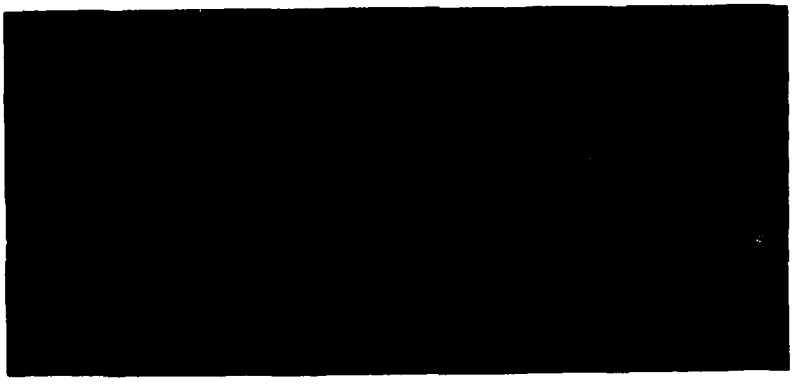

Figure 9. Oil Flow Visualization, M = 3, α = 4°, ϕ = 90°

Figure 10. Oil Flow Visualization, M = 3, α = 4°, ϕ = 180°

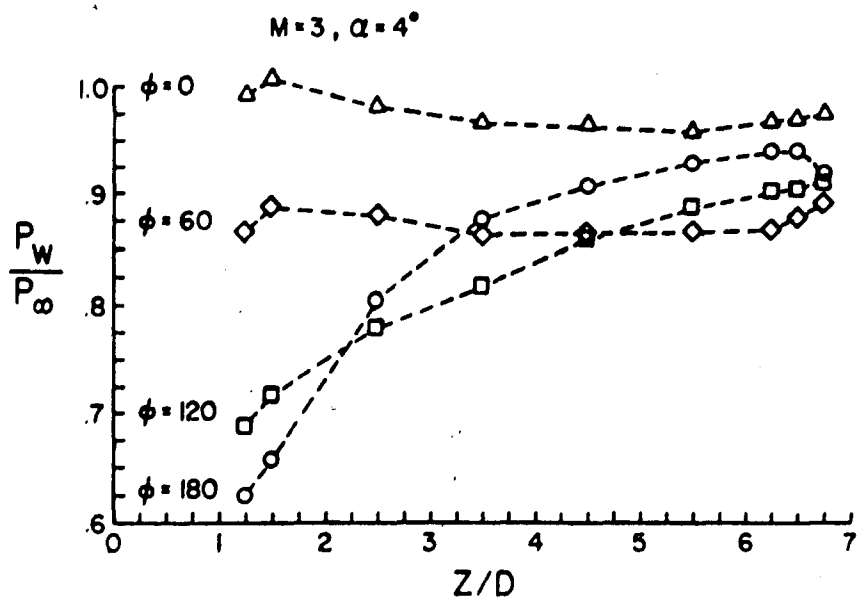

Figure 11. Wall Static Pressure Distribution, M = 3, α = 4°

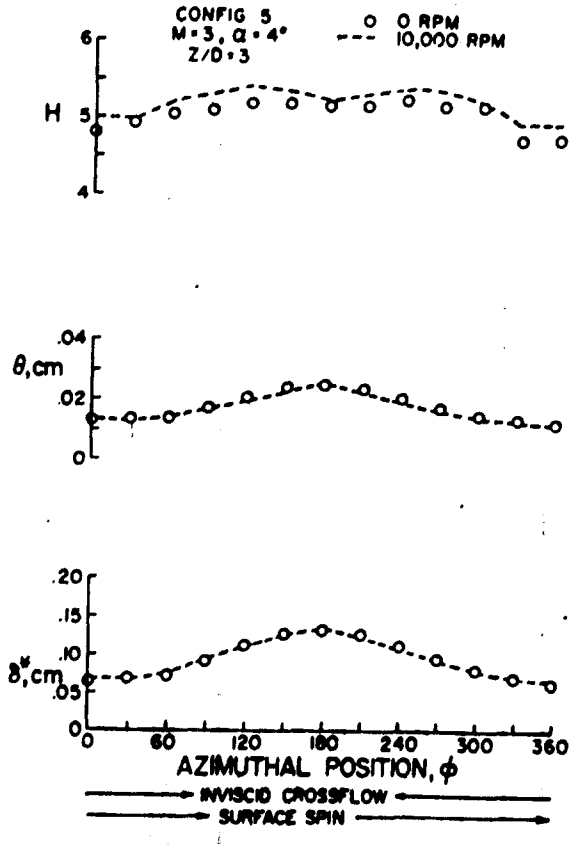

Figure 12. Integral Properties of the Boundary Layer, Z/D = 3.0

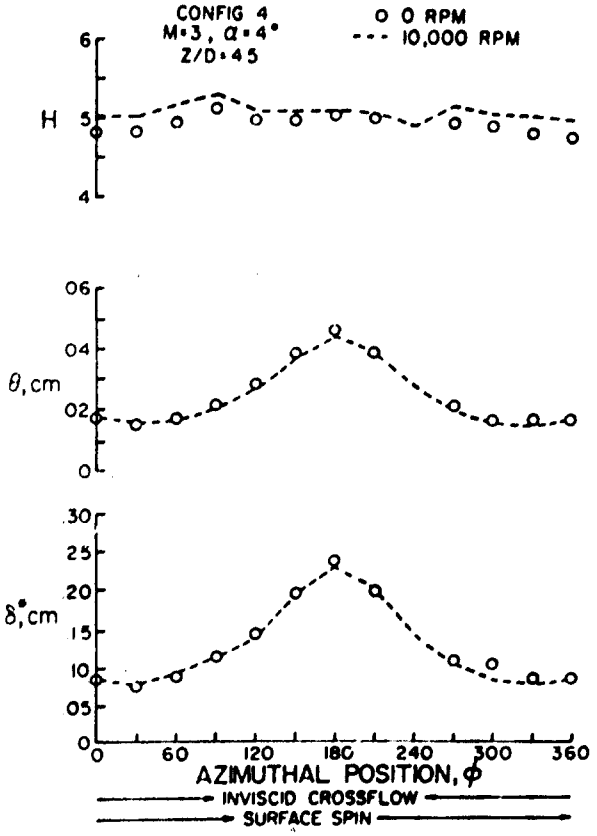

Figure 13. Integral Properties of the Boundary Layer, Z/D = 4.5

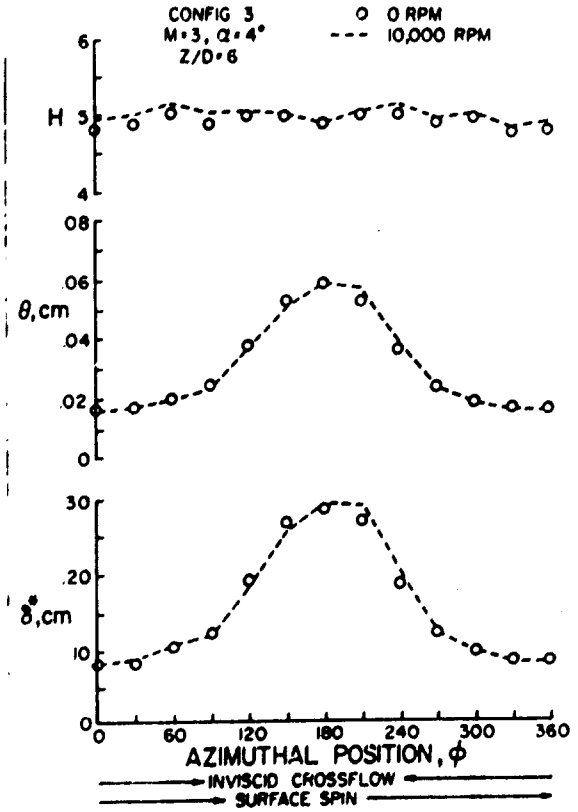

Figure 14. Integral Properties of the Boundary Layer, Z/D = 6.0

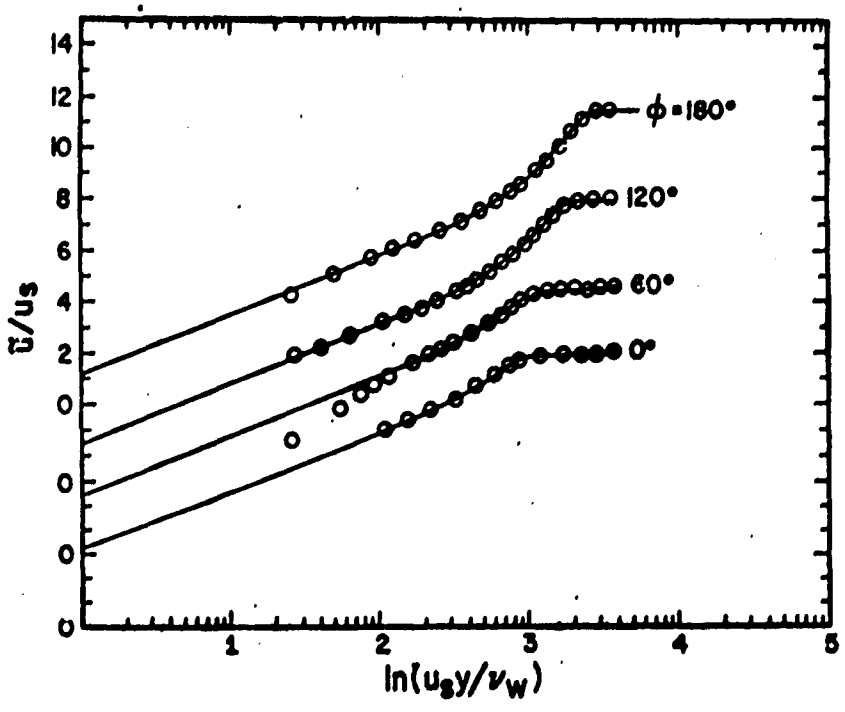

Figure 15. Velocity Profiles in Law-of-the Wall Coordinates (Z/D = 6.0, ω = 0)

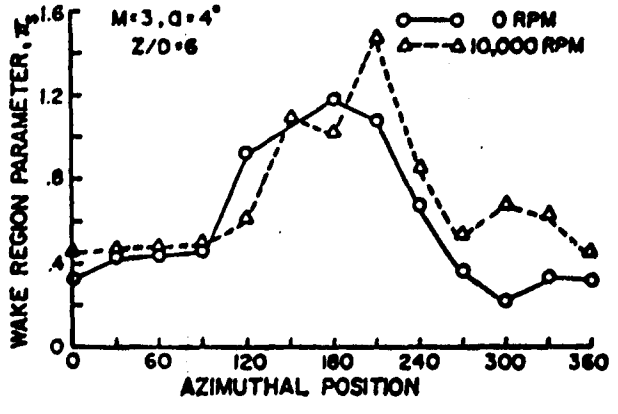

Figure 16. Wake Region Parameter, Π_s, Versus Azimuthal Position (Z/D = 6.0, ω = 0)

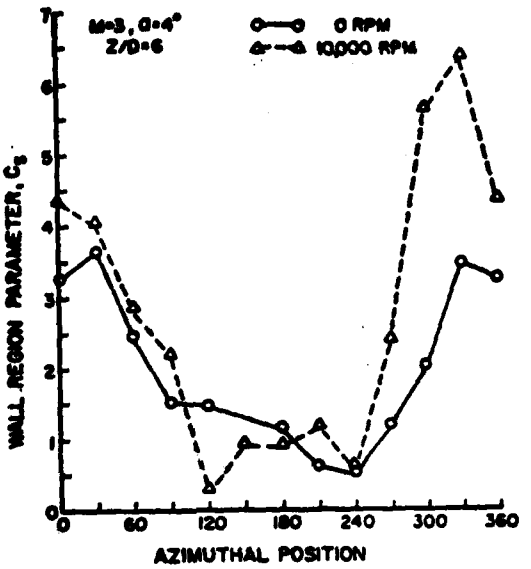

Figure 17. Wall Region Parameter, C_s, Versus Azimuthal Position ($Z/D = 6.0$, $\omega = 0$)

LIST OF SYMBOLS

C_s	law of the wall profile parameter
D	diameter of model, 5.08 cm
L	reference length, 2.54 cm
T	temperature
u	longitudinal velocity component
u_s	a velocity scale parameter
u_τ	wall shear velocity = $(\tau_w/\rho_w)^{\frac{1}{2}}$
$\tilde{u}$	transformed velocity [see equation (2)]
y	coordinate normal to surface
β	$(T_{aw} - T_w)/(T_{t_e} - T_w)$
δ	boundary layer thickness
δ_s	boundary layer thickness parameter
κ	Prandtl mixing length constant ~ 0.4
ν	kinematic viscosity
Π_s	law of the wake profile parameter
ρ	density

Subscripts

aw	adiabatic wall
e	edge of the boundary layer
t	total temperature
w	wall

DISTRIBUTION LIST

No. of Copies	Organization
12	Commander Defense Documentation Center ATTN: DDC-TCA Cameron Station Alexandria, VA 22314
1	Commander US Army Materiel Development and Readiness Command ATTN: DRCDMA-ST 5001 Eisenhower Avenue Alexandria, VA 22333
1	Commander US Army Aviation Systems Command ATTN: DRSAV-E 12th and Spruce Streets St. Louis, MO 63166
1	Director US Army Air Mobility Research and Development Laboratory Ames Research Center Moffett Field, CA 94035
1	Commander US Army Electronics Command ATTN: DRSEL-RD Fort Monmouth, NJ 07703
4	Commander US Army Missile Command ATTN: DRSMI-R DRSMI-RDK Mr. R. Deep Mr. R. Becht Dr. D. Spring Redstone Arsenal, AL 35809
1	Commander US Army Tank Automotive Development Command ATTN: DRDTA-RWL Warren, MI 48090
2	Commander US Army Mobility Equipment Research & Development Command ATTN: Tech Docu Cen, Bldg. 315 DRSME-RZT Fort Belvoir, VA 22060
1	Commander US Army Armament Command Rock Island, IL 61202
3	Commander US Army Picatinny Arsenal ATTN: SARPA-FR-S-A Mr. D. Mertz Mr. E. Falkowski Mr. A. Loeb Dover, NJ 07801
1	Commander US Army Jefferson Proving Ground ATTN: STEJP-TD-D Madison, IN 47250
1	Commander US Army Harry Diamond Labs ATTN: DRXDO-TI 2800 Powder Mill Road Adelphi, MD 20783
1	Director US Army TRADOC Systems Analysis Activity ATTN: ATAA-SA White Sands Missile Range NM 88002
1	Commander US Army Research Office P. O. Box 12211 Research Triangle Park NC 27709

DISTRIBUTION LIST

No. of Copies	Organization
2	Commander David W. Taylor Naval Ship Research & Development Ctr ATTN: Dr. S. de los Santos Mr. Stanley Gottlieb Bethesda, MD 20084
1	Commander US Naval Surface Weapons Cen ATTN: Dr. T. Clare, Code DK20 Dahlgren, VA 22448
4	Commander US Naval Surface Weapons Cen ATTN: Code 312, S. Hastings Code 313, Mr. R. Lee Mr. W. Yanta Mr. R. Voisinet Silver Spring, MD 20910
2	Director National Aeronautics and Space Administration Langley Research Center ATTN: MS 185, Tech Lib MS 161, D. Bushnell Langley Station Hampton, VA 23365
1	Douglas Aircraft Company McDonnell Douglas Corp ATTN: Dr. Tuncer Cebeci 3855 Lakewood Boulevard Long Beach, CA 90801
1	Sandia Laboratories ATTN: Dr. F. G. Blottner P. O. Box 5800 Albuquerque, NM 87115
2	Princeton University James Forrestal Research Center Gas Dynamics Laboratory ATTN: Prof. S. Bogdonoff Prof. I. Vas Princeton, NJ 08540
1	University of California Department of Mechanical Eng ATTN: Prof. H. A. Dwyer Davis, CA 95616
1	University of Delaware Mechanical and Aerospace Engineering Department ATTN: Dr. J. E. Danberg Newark, DE 19711
2	University of Virginia Dept of Aerospace Engineering and Engineering Physics ATTN: Prof. I. Jacobson Prof. J. B. Morton Charlottesville, VA 22904
	Aberdeen Proving Ground
	Marine Corps Ln Ofc Dir, USAMSAA